Optical microscopy using a glass microsphere for metrology of sub-wavelength nanostructures

Hui Yang[*] and Martin A.M. Gijs

Laboratory of Microsystems, École Polytechnique Fédérale de Lausanne, CH-1015 Lausanne, SWITZERLAND

Abstract

A technique that allows direct optical imaging of nanostructures and determines quantitatively geometric nanofeatures beyond the classical diffraction limit by using high-refractive index glass microspheres is introduced. The glass microsphere is put on a nanostructure that is immersed in oil and collects the sample's near-field evanescent wave and transforms it into a propagating one, thereby generating a magnified image in the far-field which is recorded by a conventional oil-immersion microscope objective. Experimental results on nanostructures demonstrates a resolution of ~ $\lambda/4$ - $\lambda/7$, where λ is the illumination wavelength, by using a 60 μm glass microsphere and a normal wideband halogen lamp as illumination source. A two-dimensional numerical numerical study of the light propagation through a glass microsphere using finite element method (FEM) is performed, providing key insight into the microsphere's superior imaging capability.

1

*Corresponding author. Tel: +41-21-6936815; fax: +41-21-6935950. *E-mail address*:

hui.yang@epfl.ch

5

Introduction

The conventional optical microscope is one of the most important scientific instruments; it has

been used extensively for research in different branches of science for decades. However, it has a

strict limitation in spatial resolution. Due to the diffraction of light, the minimum size that can be

resolved in a sample is around one half of the wavelength of illumination or a few hundred

nanometers in the visible(infrared) wavelength region, this constraint of optical microscopy is

well-known as Abbe's diffraction limit [1]. How to break the diffraction barrier has become the

vital concern for achieving super-resolution. It is well known that microspheres that are

significantly larger than the illumination wavelength can be treated as focusing lenses [2-4], as

the illumination light can be highly focused by the microsphere into an extremely small region,

i.e. a photonic nanojet. The photonic nanojet has high field enhancement, sub-wavelength

transverse dimension, low divergence, and is located in immediate vicinity of the rear surface of

the microsphere [5-9]. On a fundamental level, the focus spot size, i.e. the transverse dimension

of a photonic nanojet for a microsphere lens, is at the basis of the super-resolution imaging

capability of microsphere-based optical microscopy [10-13]. Therefore, microspheres hold great

potential to break the diffraction limit and achieve super-resolution [14-16]. The imaging

capability of a microsphere depends on parameters, including the refractive index ratio of the

microsphere and its surrounding medium, the illumination wavelength, and its size [17-19]. By

carefully tuning these parameters, the microspheres show the capability of imaging nano-objects

1 with super-resolution. Moreover, microspheres formed from melts yield exquisitely smooth

2 surfaces that provide superior optical characteristics. Such microspheres are inexpensive and are

3 available in a range of sizes and materials [20]. These properties make the microspheres suitable

4 for achieving super-resolution imaging. In our study, the use of barium titanate glass

5 microspheres for facile and affordable super-resolution imaging of nanometer size objects is

6 proposed and the resolution capability of the microsphere is studied numerically by a FEM

7 simulation of the photonic nanojet phenomenon.

8

9 Experimental

10 The high-refractive index ($n_p = 1.92$) barium titanate glass microspheres with diameter of 60 μm

11 is used as microlenses to achieve imaging of nanostructures with super-resolution, and the

12 potential of the technique is demonstrated by resolving the sub-diffraction features of

13 nanopatterns. In the experiments, the microspheres are simply put on a sample, projecting the

14 sample's near-field nano-features into the far-field, generating a magnified virtual image. Both

15 the microsphere and the sample are immersed in oil. A halogen lamp with full visible spectrum

16 (400-750 nm) is used as the illumination source. A 63× oil immersion objective with numerical

17 aperture (NA) of 1.4 is used for illumination and observation at the same time. When looking

18 through the microsphere into its virtual image plane, sub-diffraction-limited features become

19 visible and can be imaged by using a conventional optical microscope mounted with a CCD

20 camera. A schematic of the microsphere combined with the microscope objective is illustrated in

21 Fig. 1. In this case, the optical super-resolution imaging can be achieved in a simple

22 implementation just by locating the microsphere on the object surface of interest.

23
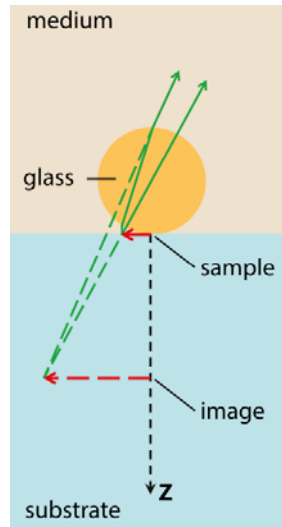
Figure 1. Diagram of the virtual image formation by a microsphere nanoscope. A microsphere is located on top of the sample and generates a virtual image in the far-field.

Results and discussion

To demonstrate enhanced spatial resolution, we investigate the super-resolution capability of the microspheres with diameter of 60 μm on subdiffraction nanofeatures. Fig. 2 shows scanning electron microscope (SEM) graph (see Fig. 2(a)) and optical images of 120 nm-wide silicon line structures, with 100 nm inter-spacing. For comparison, the optical images obtained by the oil immersion objective along and with a glass microsphere are shown in Fig. 2(b) and 2(c), respectively. The lateral resolution limit of a conventional optical microscope is expressed as Rayleigh resolution$_{x-y}$ = 0.61λ/NA [21]. For the oil immersion objective used in the experiments, this limit is estimated to be 174 nm for the lowest visible wavelength λ = 400 nm. When no microsphere is used, the oil immersion objective alone cannot resolve line structures of Fig. 2(a) indeed (see Fig. 2(b)). On the other hand, when the microsphere is placed on top of the sample, the individual lines with width ~ 100 nm are clearly resolved (see Fig. 2(c)), demonstrating an experimental resolution between λ/4 (λ = 400 nm) and λ/7 (λ = 750 nm) in the visible spectrum

4

range. The virtual image is magnified by a factor of 2.8. A narrow bandwidth filter in front of the halogen lamp can actually help to narrow down the illumination spectral range, minimize the chromatic aberration and enhance the image contrast. It is envisaged that a resolution better than 100 nm can be achieved with a band-pass filter in the blue wavelength region. Moreover, the sub-diffraction limited features are resolved the best at the center of the microsphere nanoscope. We define the diameter of the area on the image plane without clear distortion as the field-of-view (FOV), it increases with the feature size of the nanopatterns (see Fig. 3), for ~100 nm patterns, the FOV is ~15 μm, while it is ~ 30 μm for 200 nm patterns. Since we obtain a magnified circular imaging area without distortion of typically 15 μm in diameter in Fig 3(a), this corresponds to a (non-magnified) sample area of 22.5 μm^2. It should be noted that these images are taken using a commonly used 63× oil immersion objective with NA = 1.4, which is able to monitor a sample over a FOV of ~143 μm × 107 μm for observing simultaneously an ensemble of 5 microsphere nanoscopes, this yields an effective sample super-resolution imaging area of 112.5 μm^2.
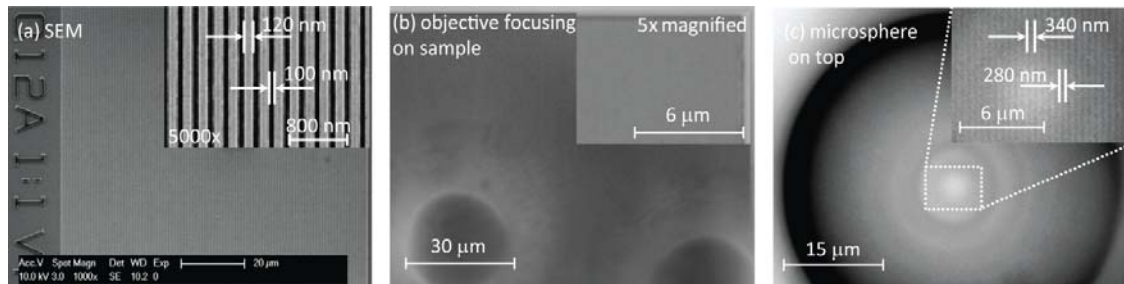

Figure 2. Measurement of nanometer-size objects by both SEM (a) and by optical microscopy (b, c) using a microsphere and 63× oil immersion objective (NA = 1.4). (a) The SEM image is obtained from an etched silicon nanostructure having a 120 nm-wide line pattern with 100 nm inter-spacing. (b) The focal plane of the oil immersion objective coincides with the nanopatterns. Hence, on this picture, the microspheres are out of focus. The insert is a 5× magnified image on an area outside the microsphere, clearly showing that the conventional oil immersion objective cannot resolve the nanopatterns with a feature size of ~ 100 nm. (c) The corresponding optical image obtained by focusing through the microsphere onto the virtual image plane. It shows that objects are magnified 2.8× due to the use of the microsphere and the ~100 nm features are best resolved in a central region of the microsphere (~ 15 μm range).

1

2
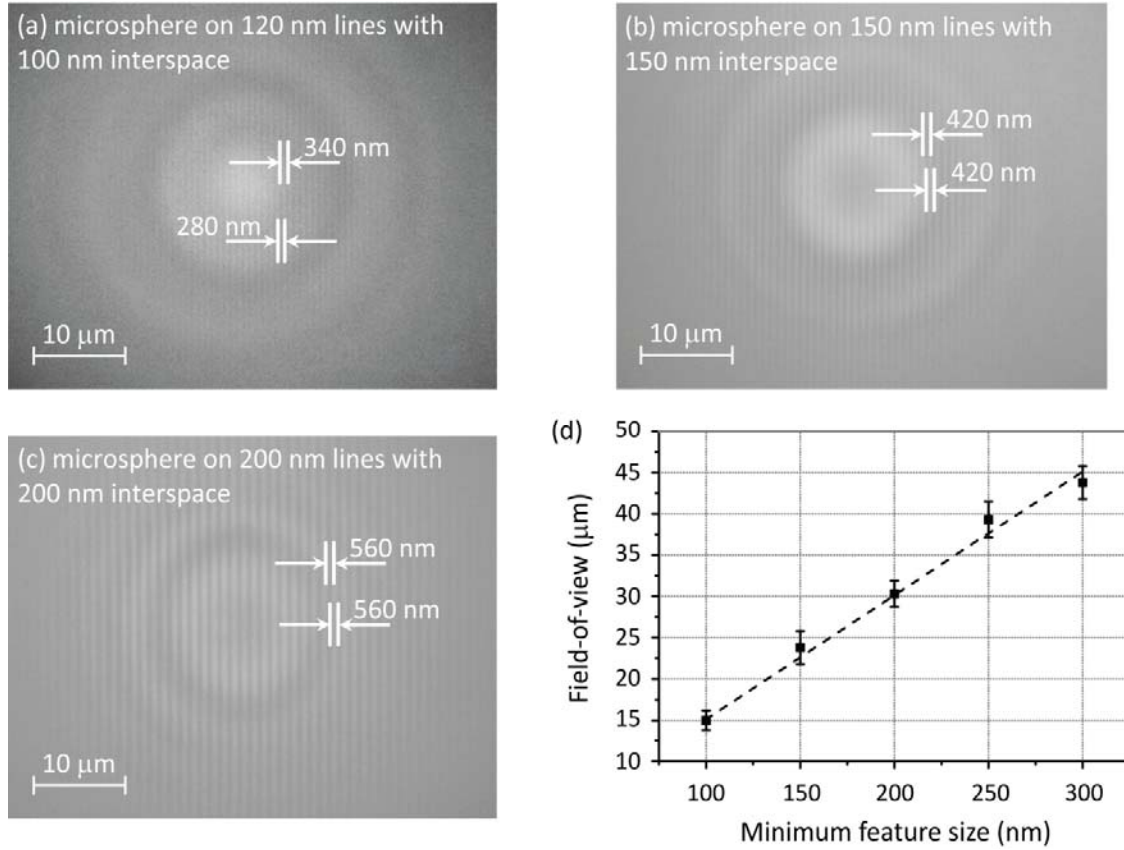
Figure 3. Measurement of nanopatterns with different feature sizes obtained by optical microscopy using a 60 μm microsphere nanoscope and a 63× oil immersion objective (NA = 1.4), showing that the FOV, over which the line pattern is visible without clear distortion, increases with the feature size that is to be resolved. (a,b,c) Images obtained through a microsphere nanoscope on 120 nm-wide lines with 100 nm interspacing, 150 nm-wide lines with 150 nm interspacing, as well as 200 nm-wide lines with 200 nm interspacing, respectively. (d) The experiment shows that the FOV linearly increases with the feature size of the nanopattern beneath the microsphere. The data are obtained from 50 measurements, points represent the average and error bars the variance, while dashed line is guide to the eye.

12

13   We further perform a FEM simulation to study the electromagnetic field distribution in the

14   vicinity of a dielectric microsphere and provide insight into the mechanism of its superior

15   imaging capability. In particular, the RF module in the FEM software COMSOL Multiphysics

6

1   (version 4.2) is used to study the electric fields from Maxwell's vector wave equation in the glass

2   microsphere ($n_p = 1.92$) and the surrounding oil ($n_m = 1.52$). Hence the governing equation is

3
$$\nabla \times \mu_r^{-1}(\nabla \times E) - k_0^2 \left(\varepsilon_r - \frac{j\sigma}{\omega \varepsilon_0} \right) E = 0 \tag{1}$$

4   where μ_r is the relative permeability, ε_r is the relative permittivity, ε_0 is the vacuum permittivity, σ

5   is the electric conductivity, ω is the angular frequency and k_0 is the free-space wave number and

6    $k_0 = \omega \sqrt{\mu_0 \varepsilon_0}$. Maxwell's equations are solved in all the sub-domains of different materials in the

7   model. For the refractive index model, the assumptions based on the material properties are $\mu_r =$

8    $1, \sigma = 0$ and $\varepsilon_r = n^2$. Equation (1) is reduced to

9
$$\nabla \times (\nabla \times E) - k_0^2 n^2 E = 0 \tag{2}$$

10   where n is the refractive index of the material. No electromagnetic loss in the media further

11   constrains the index from having an imaginary part. A harmonic propagation analysis with free

12   space wavelength of 600 nm is used to solve the dependent variable E_z. The mathematical model

13   is incomplete without adding constraints that actually introduce continuity or discontinuity in the

14   electric field solutions at the mesh nodes in the interface between two media. In the model, the

15   scattering boundary condition is used at all exterior boundaries, except an electric field is set on a

16   boundary 2 μm away from the microsphere surface as the illumination source. All the interior

17   boundaries are of course mandate continuous solutions. The point on the rear-surface of the

18   microsphere which is furthest away from the illumination source is set as the origin of the model.

19   To solve the wavelength finely enough with the mesh, the maximum element size of the

20   triangular mesh is chosen as one eighth of the wavelength in the medium. After the model is

21   solved, the distribution of the light intensity is obtained by multiplying the electric field by its

22   complex conjugate, giving the result of Fig. 4(a). From the simulation result, the microsphere

23   holds the capability to focus the radiation into an extremely small region with a waist smaller than

24   the diffraction limit and enhances the signal on the rear-side of the microsphere, effectively

1   producing the photonic nanojet. On a fundamental level, the strongly reduced transverse

2   dimension of the photonic nanojet directly indicates the super-resolution capability of the

3   microsphere nanoscope. Fig. 4(b) shows the calculated focal waist of the photonic nanojet

4   normalized by the wavelength, as function of the microsphere diameter. When the size of the

5   microsphere decreases, the focal waist of the nanojet decreases as well, and the photonic nanojet

6   moves to the rear-surface of the microsphere. When the nanojet is formed close to the

7   microsphere surface, i. e. close to the sample, this will be beneficial for the resolution and

8   magnification. The position of the photonic nanojet is decided by the relationship between the

9   size of the microsphere and the refractive indices of the dielectric materials. By properly selecting

10   the optical properties of the microsphere material and its size, it is possible to optimize the setup

11   and find conditions that lead to the minimum focal waist of the nanojet, which corresponds to

12   optimum super-resolution capability. In the conventional optical microscopy, the Rayleigh

13   resolution can be calculated by $1.22\lambda/2NA$, our super-resolution imaging setup (microsphere

14   together with the $63\times$ oil immersion objective) verifies a resolution of 100 nm with illumination

15   wavelength 400-750 nm and a magnification factor of $2.8\times$. Therefore, our setup would permit a

16   resolution that would be provided by a hypothetical (as non-existing) $176\times$ microscope objective

17   with NA of 2.4-4.6.
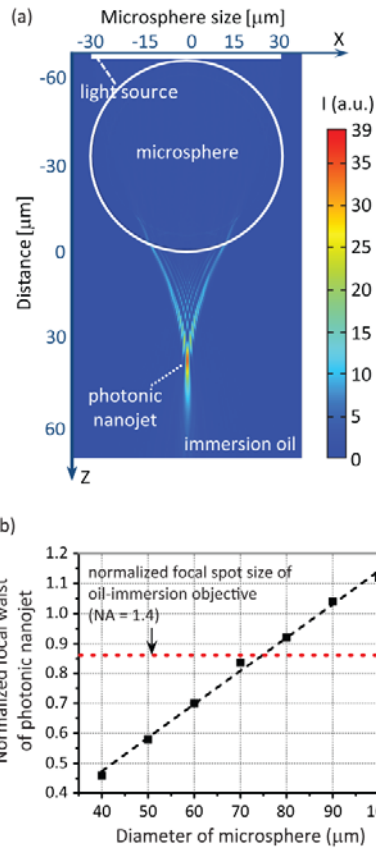
Figure 4. FEM simulation of the light propagating through a microsphere which is immersed in oil. (a) Optical intensity distribution clearly indicates a photonic nanojet generated by the microsphere which is illuminated by a plane wave. (b) The focal waist of the photonic nanojet normalized by the illumination wavelength as function of the microsphere diameter. The squares are values obtained from the simulation and the dashed line is guide to the eye. The dotted line corresponds to the normalized focal spot size of an oil immersion objective with NA of 1.4.

When a microsphere is put on top of a sample, the illuminating light passes through the microsphere and is focused by the microsphere. During this process, a photonic nanojet with width small than the diffraction limit is generated. The nanojet arrives on the sample surface and illuminates the area below the microsphere at a high intensity and a high resolution, beyond the diffraction limit. Moreover, from the Maxwell's equations, the wave vector equation for the light propagating in a microsphere with refractive index n_p can be expressed as

$$k_x^2 + k_y^2 + k_z^2 = \frac{4\pi^2 n_p^2}{\lambda^2} \tag{3}$$

When the microsphere is used as a solid immersion lens, the resolution defined by the classical Abbe's diffraction limit is

$$\Delta \approx \frac{\pi}{\sqrt{k_x^2 + k_y^2 + k_z^2}} = \frac{\lambda}{2n_p} \tag{4}$$

for the glass microsphere with n_p = 1.92, the resolution Δ of a solid immersion lens is λ/3.8. However, a resolution between λ/4 (λ = 400 nm) and λ/7 (λ = 750 nm) was obtained from previous experimental study when using white-light illumination, indicating that when the focused incident light illuminates the sample surface, the microsphere re-collects the light scattered or reflected by the sample and converts the high spatial frequency evanescent waves into propagating waves that can be collected by far-field imaging. The nanojet generated via the microsphere provides enough energy coupling to enable far-field imaging [14, 22]. Therefore, the microsphere plays a dual role for super-resolution imaging, which is (i) to generate the photonic nanojet by the microsphere for super-resolution sample illumination and (ii) to convert the high spatial-frequency evanescent waves into magnified propagating waves for far-field detection.

The object-microsphere distance plays a very important role in the super-resolution imaging [23]. The z-component of the wave vector k_z can be expressed as follows

$$k_z = \sqrt{n^2\omega^2 c^{-2} - k_x^2 - k_y^2} \tag{5}$$

which becomes imaginary, leading to exponential damping, when $k_x^2 + k_y^2 > n_p^2\omega^2 c^{-2}$ in the microsphere material with refractive index n_p, and when $k_x^2 + k_y^2 > n_m^2\omega^2 c^{-2}$ in the liquid with refractive index n_m. A wave that is propagating in the microsphere can be evanescent in the liquid,

and in this case the distance d between the object and the microsphere needs to be limited, resulting in the condition

$$|d| \leq \frac{1}{\sqrt{k_x^2 + k_y^2 - n^2 \omega^2 c^{-2}}} \tag{6}$$

From Equation (6) it becomes clear that, even if there is a distance between the sample and the microsphere, some of the evanescent waves that contain high spatial-frequencies can still be collected by the microsphere. However, the sub-diffraction-limit frequencies that can be collected by the microsphere are dramatically reduced as the distance d increases. In practice the distance between sample and microsphere surfaces should be on the same order as the light wavelength to obtain a significant image resolution improvement.

Conclusion

We have reported super-resolution imaging of nanostructures with sub-diffraction feature sizes by using a microsphere nanoscope in combination with a conventional immersion objective. The experiments performed in oil with white-light illumination demonstrate an experimental resolution between $\lambda/4$ (λ = 400 nm) and $\lambda/7$ (λ = 750 nm) in the visible spectrum range with a magnification factor of 2.8. A large FOV (30 μm when using a 60 μm microsphere for imaging of nanostructure with feature size of 200 nm) is obtained as well. A numerical study using FEM is performed to study the light propagation through the microsphere nanoscope. The results shows that the microsphere highly focuses the light into the photonic nanojet and the super-resolution capability of the microsphere is dependent on the focal waist of the nanojet, correspondingly, dependent on the size of the microsphere itself. Due to the straightforwardness of this approach, the glass microsphere together with a conventional optical microscope can be widely used for

nanometrology and imaging nano-objects of biological importance, such as viruses and localized

proteins in cells.

Acknowledgement

References

[1]. L. Novotny, B. Hecht, Principles of Nano-Optics, second ed., Cambridge University Press, 2012.

[2]. H. Yang, M. A. M. Gijs, Microtextured substrates and microparticles used as *in situ* lenses for on-chip immunofluorescence amplification, Anal. Chem. 85 (2013) 2064-2071.

[3]. J. P. Brody, S. R. Quake, A self-assembled microlensing rotational probe, Appl. Phys. Lett. 74 (1999) 144-146.

[4]. H. Yang, M. Cornaglia, M. A. M. Gijs, Photonic nanojet array for fast detection of single nanoparticles in a flow, Nano Lett. (2015) doi: 10.1021/nl5044067.

[5]. A. Heifetz, S.-C. Kong, A. V. Sahakian, A. Taflove, V. Backman, Photonic nanojets, J. Comput. Theor. Nanosci. 6 (2009) 1979-1992.

[6]. M.-K. Kim, T. Scharf, S. Mühlig, C. Rockstuhl, H. P. Herzig, Engineering photonic nanojets, Opt. Express 19 (2011)10206-10220.

[7]. A. V. Itagi, W. A. Challener, Optics of photonic nanojets, J. Opt. Soc. Am. A 22 (2005) 2847-

2858.

[8]. P. Ferrand, J. Wenger, A. Devilez, M. Pianta, B. Stout, N. Bonod, E. Popov, H. Rigneault, Direct imaging of photonic nanojets, Opt. Express 16 (2008) 6930-6940.

[9]. H. Rigneault, J. Capoulade, J. Dintinger, J. Wenger, N. Bonod, E. Popov, T. W. Ebbesen, P.-F. Lenne, Enhancement of single-molecule fluorescence detection in subwavelength apertures, Phys. Rev. Lett. 95 (2005) 117401.

[10]. Z. Wang, W. Guo, L. Li, B. Luk'yanchuk, A. Khan, Z. Liu, Z. Chen, M. Hong, Optical virtual imaging at 50 nm lateral resolution with a white-light nanoscope, Nat. Commun. 2 (2011) doi:10.1038 / ncomms1211.

[11]. Z. B. Wang, N. Joseph, L. Li, B. S. Luk'yanchuk, A review of optical near-fields in particle/tip-assisted laser nanofabrication, J. Mech. Eng. Sci. 224 (2010) 1113-1127.

[12]. A. Darafsheh, G. F. Walsh, L. D. Negro, V. N. Astratov, Optical super-resolution by high-index liquid-immersed microspheres, Appl. Phys. Lett. 101 (2012) 141128.

[13]. Y. E. Geints, E. K. Panina, A. A. Zemlyanov, Control over parameters of photonic nanojets of dielectric microspheres, Opt. Commun. 283 (2010) 4775-4781.

[14] L. Li, W. Guo, Y. Yan, S. Lee, T. Wang, Label-free super-resolution imaging of adenoviruses by submerged microsphere optical nanoscopy, Light Sci. Appl. 2 (2013) doi:10.1038/lsa.2013.60.

[15]. S. Lee, L. Li, Y. Ben-Aryeh, Z. Wang, W. Guo, Overcoming the diffraction limit induced by microsphere optical nanoscopy, J. Opt. 15 (2013) 125710.

[16]. H. Yang, N. Moullan, J. Auwerx, M. A. M. Gijs, Super-resolution biological microscopy using virtual imaging by a microsphere nanoscope, Small 10 (2014) 1712-1718.

[17]. C. Kuang, Y. Liu, X. Hao, D. Luo, X. Liu, Creating attoliter detection volume by microsphere photonic nanojet and fluorescence depletion, Opt. Commun. 285 (2012) 402-406.

[18]. D. Gérard, J. Wenger, A. Devilez, D. Gachet, B. Stout, N. Bonod, E. Popov, H. Rigneault, Strong electromagnetic confinement near dielectric microspheres to enhance single-molecule fluorescence, Opt. Express 16 (2008) 15297-15303.

1   [19]. J. J. Wang, D. McCloskey, J. F. Donegan, Optimization of parameters of photonic nanojet

2   generated by dielectric microsphere for "laser nanojet" SNOM, Proc. SPIE 8321 (2011) 83213Z.

3   [20]. D. C. Kim, K. P. Armendariz, R. C. Dunn, Integration of microsphere resonators with

4   bioassay fluidics for whispering gallery mode imaging, Analyst 138 (2013) 3189-3195.

5   [21]. P. J. Shaw, D. J. Rawlins, The point-spread function of a confocal microscope: its

6   measurement and use in deconvolution of 3-D data, J. Microsc. 163 (1991) 151-165.

7   [22]. X. Hao, C. Kuang, X. Liu, H. Zhang, Y. Li, Microsphere based microscope with optical

8   super-resolution capability, Appl. Phys. Lett. 99 (2011) 203102.

9   [23]. S. Lee, L. Li, Z. Wang, W. Guo, Y. Yan, T. Wang, Immersed transparent microsphere

10   magnifying sub-diffraction-limited objects, Appl. Opt. 52 (2013) 7265-7270.

11